Journal of Magnetics 15(4), 221-224 (2010) DOI: 10.4283/JMAG.2010.15.4.221

GMI Magnetic Field Sensor Based on a Time-coded Principle

Xuan-Huu Cao and Derac Son*

Department of Physics, Hannam University, Daejeon 306-791, Korea

(Received 30 July 2010, Received in final form 6 September 2010, Accepted 7 September 2010)

A laboratory sensor model was designed, constructed, and tested based on a newly proposed working principle of magnetic field detection. The principle of sensing employed a time-coded method in correlation with exploiting the advantageous features of the GMI effect. The sensor demonstrated a sensitivity of 10 μs/μT in the field range of ±100 μT. The sensing element in the form of an amorphous thin wire, 100 μm in diameter × 50 mm long, was fit into a small field modulation coil of 60 mm length. At a magnetic field modulation in the range of hundreds of Hz, the change in time interval of two adjacent GMI voltage peaks was linearly related to the external magnetic field to be measured. This mechanism improved the sensor linearity of the GMI sensor to better than 0.2% in the measuring range of ±100 μT.

Keywords : time-coded, magnetic field sensor, GMI, amorphous wire

1. Introduction

Giant magneto-impedance (GMI) phenomenon was first observed in the 1930s, but without attracting much attention. Since Panina and Mohri reported the GMI effect in Co-Fe-Si-B soft magnetic amorphous wires in 1994 [1, 2], the GMI effect has provided a novel method for detecting low magnetic field with very high sensitivity. Recent studies on the GMI effect have exhibited the possibility of fabricating magnetic field sensors with high performance [3-6]. Due to their high sensitivity, fast response, good stability, low power consumption, and easy miniaturization, GMI sensors show great potential as the next generation of magnetic sensors for low magnetic field detection [7-9].

In the development of GMI sensors [3], most technological applications are related to micro-sensors in which the principle of operation is based on the static field dependence of the magneto-impedance. In general, when the GMI curve is measured in a magnetic field, the GMI ratio profile of an amorphous wire has a typical form of a solid curve, shown in Fig. 1. As a matter of fact, there exists small hysteresis [10] (see Fig. 1) between the forward (solid line) and backward (dotted line) curves of the GMI profiles. This behavior is also called the memory effect, due to the remembered state after field removal. Obviously, this fact is more apparent when the wires are exposed to a strong enough magnetic field from the nearby electromagnets or strong permanent magnets, which leads to incorrect readout data. Nevertheless, this fact of hysteresis and/or memory effect has been neglected thus far by many authors.

To determine the relationship between the GMI ratio and the magnetic field, several previous works have presented methods for directly measuring the magnetic field using the linear region of the GMI curve. In order to obtain higher linearity, some studies presented a method of using a bias field and feedback coil for the chosen working point settled on the linear region of the GMI profile [4, 7]. Other studies have conducted a compensating item by utilizing another identical sensing element,

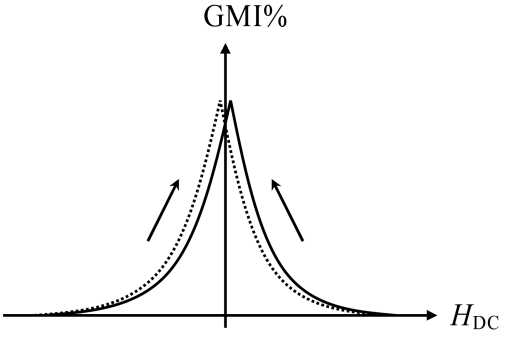

Fig. 1. GMI curves measured in a DC magnetic field.

*Corresponding author: Tel: +82-42-629-7512
Fax: +82-42-629-8313, e-mail: deracson@hnu.kr

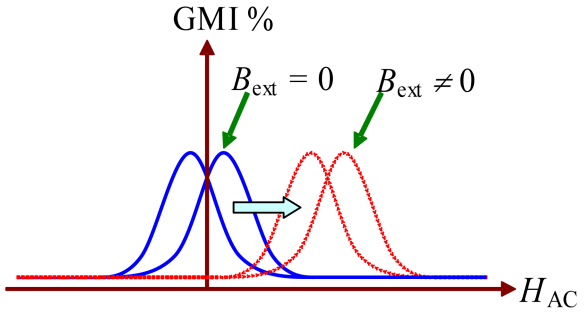

Fig. 2. GMI curve shifts corresponding in the presence of an external DC magnetic field.

consisting of a pair of GMI elements, for obtaining differentiation of the symmetric configuration [11]. Still, other authors [12, 13] have employed two coils for detecting both the magnetic field and mechanical displacement, which lead to large sensor sizes. In most cases, these conventional methods were unable to overcome the hysteresis and/or memory effects and the non-linearity of the operating points.

In an AC magnetic field, however, the GMI effect of an amorphous wire reveals an even function, showing a large hysteresis area, as shown in the solid curve in Fig. 2. When there is a presence of an external magnetic field (B_{ext}), the whole set of GMI curves are shifted from the original location to a new position, as shown by the dotted curve. Based on this finding, the present work proposes another idea, which combines the advantages of time-coded progress in [13] with the advantageous features of the sensing element's GMI effect. On the basis of this idea, this lab constructed a laboratory model of the designed sensor.

2. Operation Principle of the Designed Sensor

At the first study stage [14], a proposed laboratory model sensor was successfully constructed and tested in which the GMI signal input to the comparator was directly obtained from the output of the low pass filter. In this study, the authors proceeded upon an advanced route for improving signal linearity and stability by using a stage of differentiator right after the low pass filter, as shown in Fig. 3.

In similarity to the previous study [14], an amorphous micro-wire was employed as the active magnetic element, due to the extremely high GMI ratio [1, 2] resulted from circumferential magnetic anisotropy. As shown in Fig. 3, the amorphous wire was inserted into a magnetic field modulation solenoid, which was long enough to cover the whole of its length, and was subjected to an AC current at

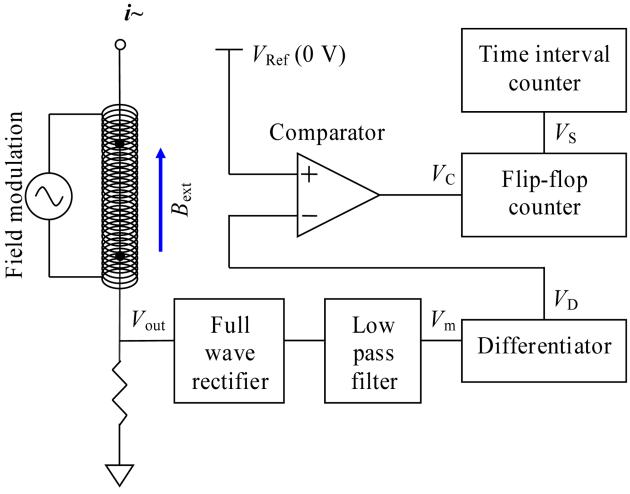

Fig. 3. Block diagram of the designed sensor.

a frequency of a few hundred kHz. The GMI ratio of the amorphous wire was obtained after the low pass filter stage.

Basically, the mode of the operation principle of the sensor is shown in Fig. 4, where the time-based progresses of V_m, V_D, V_C, and V_S are presented with respect to those in Fig. 3. According to the flux-gate principle, if the

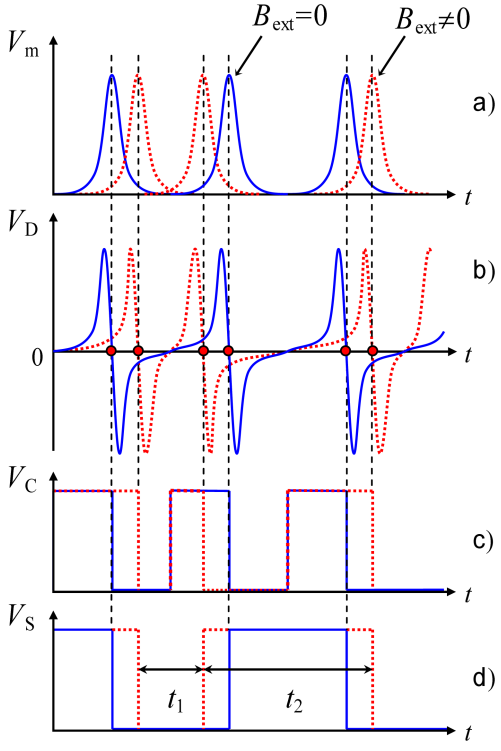

Fig. 4. Operational principle of the designed sensor: a) GMI voltage signal under modulation field, b) GMI voltage signals after differentiation stage, c) comparator output of V_D and 0-V reference, and d) final output for time interval counting.

modulation field is strong enough to induce saturation of the GMI curve, the shifts of the GMI peaks express the presence of the external field to be measured (as pointed out in Fig. 2). Fig. 4(a) presents the time-based progress of the voltage drop $V_m(t)$, which is determined from the GMI(H) curve shown in Fig. 2. Fig. 4(b) expresses the time-based progress of the differentiation $V_D(t)$ of the voltage drop $V_m(t)$. Because the GMI curves are shifted with the external magnetic field, the $V_D(t)$ signal also acts in the same way in the presence of the external field. When $H_{ext} = 0$, the V_m signal occurs in the time symmetry position (solid line curve). When $H_{ext} \neq 0$ acts along the amorphous wire axis, it brings the shift of the peaks corresponding to the external field (dotted line curve). To digitally measure time positions of the peaks of $V_m(t)$, a differentiator using an operational amplifier and voltage comparator with TTL outputs was employed. Correspondingly, TTL level changes in voltage comparator output be have the same as the shifts. Consequently, these shifts due to the external magnetic field express the change in the time interval (Δt), which is proportional to the external field. Here:

$$\Delta t = t_2 - t_1 \tag{1}$$

where t_1 and t_2 are the time interval of the first and the second half cycle of the TTL signal, respectively, as shown in Fig. 4(d). Technically, a rectangular voltage signal (V_S) was created by means of flip-flop counting from the previously TTL signal (V_C) output of the comparator, and then transferred to the final stage of time encoding for counting the time interval (Fig. 3). This progress reduced the 2f frequency signal V_C (at the comparator output) to 1f TTL signal V_S (at final output).

Therefore, this time-coded method, in combination with the advantages of the GMI effect, improved the following important application terms of the sensor: high linearity; no hysteresis; no memory effect. In addition, without the need for related electronics of the compensation items, as required in other methods, the present sensor can be advanced to a more compactable form for later manufacturing stages. The sensitivity of the sensor in this case has been defined as:

$$S = \frac{\Delta t}{\Delta B}, \tag{2}$$

where ΔB is the amount of the induction of the external magnetic field in accordance with Δt.

3. Experiment

An actual experiment was conducted following the schematic diagram shown in Fig. 3. An amorphous wire, DC-2T (Unitika Co., Japan), with a diameter of 100 μm and a length of 50 mm, was settled at the axis of a modulation coil wound from enameled copper wire. The excitation AC current fed to the amorphous wire was set at a frequency of 300 kHz. The whole set of the sensor was placed in the center of a Helmholtz coil, which produces the external DC magnetic fields along the amorphous wire axis. The triangular magnetic field created inside modulation coil has a frequency of 50 Hz and amplitude of 1.0×10^{-3} T, which was sufficient to be imposed on the external DC magnetic field and large enough to saturate the wire, respectively. The time intervals were measured by a Universal Counter HP 53131A with a resolution of 0.5 ns.

4. Results of Sensor Characteristics and Discussions

Fig. 5 presents the linearity of the sensor operated in the measured ranges of ± 100 μT. The sensitivity of the magnetic sensor calculated from Eq. (2) was 10 μs/μT, with a resolution of 15 nT, while the noise level was 3 nT (rms). Experimentally, the linearity calculated by means of the standard derivation method was 0.2% for a field range of ± 100 μT. The hysteresis and/or memory effect of the sensor was checked by examining the offset field between having and not having a strong permanent magnet (B ~ 0.2 T at surface) close to the sensor. The offset was less than one thousandth (1‰) for the full scale.

From these results, one can see that the designed sensor was operating with very high performance in the field range of ± 100 μT. As mentioned above, the results revealed improvements to important application terms of

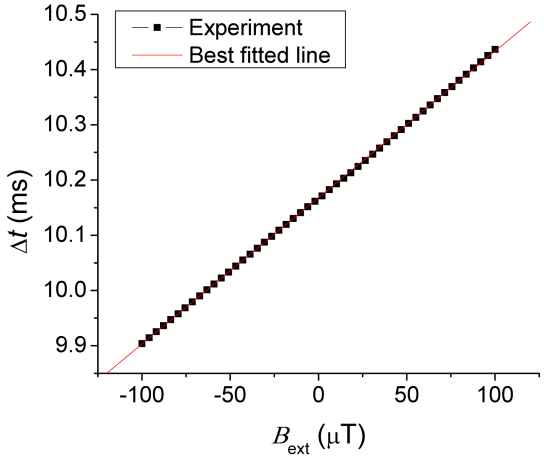

Fig. 5. Characteristics of the designed sensor in the field range of ± 100 μT.

Table 1. Comparison between the performance characteristics of the sensor in this work and in Ref. 16.

Sensor	Operating range	Resolution	Sensitivity	Linearity error	Size	Hysteresis
Ref [16]	± 80 μT	200 nT	526 mV/mT	9.6%	100 mm	1%, existed
This work	± 100 μT	15 nT	10 ms/mT	0.2%	50 mm	< 1‰, negligible

the sensor, like high linearity, no hysteresis and/or no memory effect, when compared to the other method, as previously reported [15, 16]. In addition, other features, such as operating field range, resolution, and physical dimension of the designed sensor, become clearly surpassing, even at such a preliminary stage of the currently proposed sensor. Table 1 gives the comparison of these characteristics to those previously reported Ref. [16].

One can deduce from this Table that all of the crucial characteristics for sensor applications were improved. Regarding the relative comparison of the sensitivity per mT, the present sensor was 10 ms/mT, which was 2.0×10^7 times of resolution of the counter equipment (0.5 ns), whereas that of sensor in Ref. [16] was approximately 500 mV/mT, which was 5.0×10^5 of the minimum possible measure (here it is considered as of 1.0 μV as normally). Furthermore, no bias field and related items (as shown in [15]) were needed, which lead to a reduction in size and simplification in the usage. Furthermore, the property of the maximum GMI effect reached when the longitudinally external field subjects along the wire axis bears another advantage for the directional sensor. As derived from Fig. 5, the sensor is able to sense the reverse field because of different time interval detection at the reversed field direction. In this sense, the sensor is bidirectional [17]. Certainly, the sensor will be better realized when such features as miniaturization and sensing element modification are optimized at later development stages.

5. Conclusions

A new GMI magnetic field sensor was designed, constructed, and tested based on the time-coded principle. The functional principle of the sensor operation relies on the measurement of the changes in time interval of the GMI voltage drop peaks in the presence of an external DC magnetic field. This time-coded method, in accordance with the advantages of the GMI effect, helped improve the linearity better than 0.2% and contributed to a sensitivity of 10 μs/μT and resolution of 15 nT with a low noise level of 3 nT (rms), and diminished the hysteresis and/or memory effect. The obtained study results, although only preliminary, are acceptable to proceed to the next advanced stage of further microminiaturization and size optimization, along with optimized electronics and a sensing element.

Acknowledgements

This study was supported partially by Hannam University Research Grant of 2010.

References

[1] K. Mohri, Mater. Sci. Eng. **A185**, 141 (1994).
[2] L. V. Panina, K. Mohri, K. Bushida, and M. Noda, J. Appl. Phys. **76**, 6198 (1994).
[3] K. Mohri, T. Uchiyama, L. P. Shen, C. M. Cai, and L. V. Panina, Sensor and Actuators A **59**, 1 (1997).
[4] K. Mohri, T. Uchiyama, L. P. Shen, C. M. Cai, and L. V. Panina, Sensor and Actuators A **91**, 85 (2001).
[5] G. V. Kurlyandskays, A. Garcia-Arribas, and J. M. Barandiaran, Sensor and Actuators A **106**, 234 (2003).
[6] H. Chiriac, M. Tibu, A.-E. Moga, and D. D. Herea, J. Magn. Magn. Mater. **293**, 671 (2005).
[7] Y. Honkura, J. Magn. Magn. Mater. **249**, 375 (2002).
[8] S. Yabukami, H. Mawatari, N. Horikoshi, Y. Murayama, T. Ozawa, and K. Ishiyama, J. Magn. Magn. Mater. **290**, 1318 (2005).
[9] J. Yanwei, F. Jiancheng, and H. Xuegong, S. Yujun, IEEE Trans. Magn. **34**, 1 (2008).
[10] J. P. Sinnecker, P. Tiberto, G. V. Kurlyandskaia, E. H. C. P. Sinnecker, M. Va´zquez, and A. Hernando, J. Appl. Phys. **84**, 5814 (1998).
[11] K. Mohri, T. Uchiyama, L. P. Shen, C. M. Cai, and L. V. Panin, J. Magn. Magn. Mater. **249**, 351 (2002).
[12] C. Chiriac, and H. Chiriac, Sensors and Actuators A **106**, 172 (2003).
[13] W. Heinecke, IEEE Trans. Instrum. Meas. **27**, 402 (1978).
[14] X. H. Cao and D. Son, J. Magnetics **14**, 129 (2009).
[15] J. G. Gore, G. J. Tomka, J. Milne, M. G. Maylin, P. T. Squire, and D. Atkinson, Mater. Res. Soc. Symp. Proc. **577**, 499 (1999).
[16] P. Ripka, A. Platil, P. Kaspar, A. Tipek, M. Malatek, and L. Kraus, J. Magn. Magn. Mater. **254**, 633 (2003).
[17] Carl H. Smith, Michael J. Caruso, and Robert W. Schneider, Tamara Bratland, http://www.sensorsmag.com/sensors/electric-magnetic/a-new-perspective-magnetic-field-sensing-855 (1998).